Fermi National Accelerator Laboratory

FERMILAB-Pub-87/170-E
[E-741/CDF]

The CDF Forward/Backward Hadron Calorimeter*

S. Cihangir, F. Marchetto*, P. McIntyre, T. Meyer, and R. Webb
Physics Department
Texas A&M University
College Station, Texas 77843

July-August 1987

*Submitted to Nucl. Instrum. Methods A

Operated by Universities Research Association Inc. under contract with the United States Department of Energy

THE CDF FORWARD/BACKWARD HADRON CALORIMETER

S. Cihangir, F. Marchetto*, P. McIntyre, T. Meyer, R. Webb

Physics Department
Texas A&M University
College Station, Texas 77843

ABSTRACT

The forward/backward hadron calorimeter of the Collider Detector at Fermilab (CDF) is composed of proportional tube chambers and steel plates. It is designed to cover a pseudorapidity region of $2.2 \leq |\eta| \leq 4.2$. The readout of this calorimeter is accomplished through sensing the induced charge pulses produced on the chamber's cathode in response to a hadronic cascade shower. We describe the main features of these chambers and present the results of performance tests on the first group of chambers produced.

I. INTRODUCTION

The Collider Detector at Fermilab (CDF) is a large multipurpose spectrometer which was designed to study the details of the physics processes involved in high energy proton-antiproton collisions at a center-of-mass energy of 2 TeV. Various components of the detector are described elsewhere[1]. This paper is devoted to the description and performance of the forward/backward hadron calorimeter of the CDF[2]. In Section II we explain the design and construction of the calorimeter. The performance of this calorimeter system is presented in Section III. A study to investigate the possibility of using isopropyl alcohol to prevent aging in this and other gas calorimeters of the CDF is described in Section IV.

II. CALORIMETER DESIGN AND CONSTRUCTION

The forward/backward hadron calorimeter of the CDF was designed to detect and measure the energies and positions of hadrons in the pseudorapidity range of $2.2 \leq |\eta| \leq 4.2$ with full azimuthal coverage with respect to the beam axis.

Each of the forward and backward calorimeters was segmented into four independent sections which, when stacked about the accelerator beam pipe, provide the necessary full azimuthal coverage. These calorimeter segments are each composed of 27 (213 cm x 213 cm x 5 cm) steel plates and 27 (204 cm x 196 cm x 2.5 cm) ionization chambers which are located between neighboring steel plates. One of these sections is shown in Figure 1 . The total assembly contains nearly 400 tons of steel plates and 216 ionization chambers.

The cathode surface of each of the ionization chambers has been segmented into 20 bins in pseudorapidity ($\Delta\eta = 0.1$) and 18 bins in azimuth ($\Delta\phi = 5^\circ$). The pad structure of a chamber is shown in Figure 2. Cathode pads at fixed pseudora-

pidity and azimuth on each of the 27 ionization chambers form a projective tower whose apex is the interaction point at a distance of 711 cm from the calorimeter face. The signals from each chamber pad at fixed η and ϕ are summed together to produce the total energy signal for a given projective tower.

The chambers are constructed using a custom made aluminum extrusion[3] (T-cross section) and a copper-clad, epoxy fiberglass circuit board to form the basic cell structure. Figure 3 shows the details of the chamber construction. The T-shaped extrusions are glued to an aluminum base plate yielding a panel with an open channel structure. Each channel in this structure has dimensions of 1.0 cm x 1.5 cm x 196 cm. An injection molded plastic plug[4] is afixed to each end of these channels to locate and fix the sense wires in each cell. These plugs are made of Ryton for better dimensional stability and insensitivity to the heat of soldering. A 50 μm diameter nickel flashed and gold-plated tungsten wire[5] is then stretched down the center of the cell with 240 grams of tension and soldered to each of these terminating blocks. The cell is then closed by gluing the cathode circuit to the top of this structure using a specially designed conducting epoxy[6]. The typical surface resistivity we are able to achieve using this material is in the range of 10-20 $M\Omega/$ square.

The signals on each of the 360 cathode pads of each chamber are bussed to the edge of the chamber using flat ribbon cables which are soldered directly to the cathode circuit and are terminated at the chamber's edge in a ribbon connector header (see Figure 3 for details). The chamber gas volume is then closed by installing a final aluminum cover, spaced above the cathode circuit by 0.6 cm to allow for a reserve gas volume and space for the passage of these ribbon cables and headers. The completed chamber is totally sealed with only the signal and

high voltage connections penetrating the gas volume. This construction results in a very small pad capacitance to ground (typical values for an individual pad are of order 100 pF)

In addition to the charge information available from each of the cathode pads in the calorimeter, we are able to read out the signals produced on the chamber's sense wires. Each chamber is segmented into six sections of wires for this purpose. These signals can be used to independently monitor the performance of the calorimeter and to provide information on the longitudinal development of showers in the detector.

III. TEST RESULTS

We tested the performance of the chambers with cosmic rays and in a test beam at Fermilab. In all our tests we used a chamber filling of 50% argon-50% ethane resulting in an operating range of high voltage from 1.9 KV to 2.4 KV.

The standard analog signal processing system for the CDF detector is the Fermilab RABBIT system. The details of this high speed, high density and intelligent analog data acquisition system is described in detail elsewhere[7]. For the testing of the calorimeter system described here, we employed a somewhat different readout scheme due to the limited availability of RABBIT electronics at the time these tests were conducted. The signals from each of our cathode pads were processed by a standard CDF charge integrating amplifier (CARROT). The pulse shape observed on the output of this amplifier is determined by the surface resistance of the conducting epoxy, the cathode pad capacitance and the amplifier time constant. We observed time constants in the range of 20-60 μsec in our tests of each production line chamber; however, the uniformity of this time constant

over the surface of each single chamber was observed to be constant to better than 10%.

To digitize the chamber outputs in our tests we bussed the 27 cathode pad signals for a single tower together through the depth of the calorimeter and then to the input of one of the integrating amplifiers. We then routed the outputs of these integrating amplifiers to a set of conventional CAMAC ADC's. In the case of the cosmic ray tests, we used the LeCroy 2282B (12 bit) ADC system and for the Fermilab test beam running, we used the LeCroy 2285A (15 bit) charge integrating system. By applying a 200 nsec wide gate signal to the ADC's delayed by approximately 2 μsec we were able to sample the peak pulse height of the much more slowly varying chamber signal at the output of our integrating amplifiers.

i) Cosmic Ray Test Results

During the construction of the calorimeter chambers we conducted several tests of the chambers' performance using minimum ionizing cosmic ray muons. The first of these tests was to monitor the uniformity of the decay time constant of the charge pulses on the cathode pads, as discussed earlier. Following this, we set up a cosmic ray telescope and used this to scan the entire chamber surface looking for gain variations in the chambers' response to muons. By digitizing the cathode pad signals for these muon events, we were able to verify that the chambers were uniform to better than 10% over their entire surface. Due to the small capacitance to ground provided by the cathode pads, the capacitance in the charge integrating circuit is dominated by the input capacitor in the charge amplifier. As a result, we observed little variation in the charge collected from different areas of the chamber surface during these cosmic ray tests. In making

a comparison of the chamber to chamber response to muons, we find that this variation is also less than 10%, which appears to be the limit of accuracy we can expect from this technique.

In addition to the uniformity tests, we measured the gain versus high voltage for each chamber using cosmic rays. As expected, the pulse height response of these chambers to variations in high voltage is characteristically exponential in nature and a typical gain curve is shown in Figure 4.

ii) Test Beam Measurements

The aim of the beam test was to measure the response and performance of one fully equipped quadrant of this hadron calorimeter system using the M-bottom test beam at Fermilab. The M-bottom beam offers the user a momentum analyzed beam of pions, electrons and muons in the range of 20-200 GeV/c with a characteristic momentum bite of $\approx 4\%$.

In the section that follows we describe the results of our test of the calorimeter system's linearity, the energy and the position resolutions, shower shape discrimination and other performance parameters.

a) Linearity, uniformity and energy resolution

During our run in the test beam, we recorded data at several different positions in the calorimeter using hadrons, electrons and muons in a range of beam momenta and as a function of the chamber high voltage. These data were then written onto magnetic tape for offline analysis. The beam momentum was also measured for each event using beam multiwire proportional chambers (MWPC's); thus we were able to correct for the momentum bite. The position information available

from these chambers was also used to study the inherent spatial resolution of this calorimeter.

Figure 5 shows a typical total energy distribution for incident pions of 100 GeV/c at the operating voltage of 2.1 KV. The smooth curve in this figure is the result of a Gaussian fit to the data. The results from this fitting procedure, the means and standard deviations, are used in the analysis presented here.

Figure 6 shows the average pulse height in number of equivalent particles(nep) as a function of the beam energy for one of the three locations for which we took data on the calorimeter. We chose the convention that one equivalent particle (ep) is the charge deposited by one minimum ionizing particle which traverses the entire calorimeter (27 planes). We fit the points of this plot to a straight line of the form nep=a+bE_{beam} and found that a=-1.01 ± 0.50 nep and b=0.263 ± 0.005 nep/GeV. The data are consistent with a linear response up to 200 GeV/c with no evidence for saturation in the output response of this calorimeter at the high energy end of these measurements. Using the fitting results and the energy loss per equivalent particle in the calorimeter, we calculate the observed energy to be 46% of the total hadron energy.

In our study of the resolution of the calorimeter as a function of the hadron shower energy, we have observed the expected energy dependence of (σ/E). In Figure 7 we plot $(\sigma/E)_{measured}$ versus $E_{beam}^{-1/2}$. Expressing the calorimeter's energy resolution as $\sigma/E = \alpha E^{-1/2}$, from our data we determined that $\alpha = 1.41\ GeV^{1/2}$ at $E = 200\ GeV$. If we allow σ/E to be represented by a more general polynomial of the form $A + BE^{-1/2} + CE^{-1}$, our data gives the following values for the constants: $A = 8.6 \times 10^{-2}$, B =1.13 $GeV^{1/2}$ and $C = 2.83\ GeV$.

We used the data taken at a fixed energy (50 GeV) but at different operating

voltages to study the dependence of the energy resolution on the voltage. The results of this study are shown in Figure 8 where we plot the energy resolution at various operating voltages. As this figure indicates, increasing the operating voltage of the calorimeter to 2.2 KV would result in an improvement in the value of α from 1.41 to 1.25 $GeV^{1/2}$[8].

b) Position resolution measurements

The position resolution inherent in the calorimeter was measured by comparing the location of the shower center of gravity with the impact position of the beam particle given by the beam MWPC's. The error in the impact position due to the spatial resolution of these beam chambers was of the order of a few millimeters. Since our smallest tower dimension was much larger than the resolution of the impact position, by using these chambers we were able to make a measurement of the spatial resolution of the calorimeter. Figure 9 shows the typical difference between the measured impact position and the center of gravity of the shower at the middle of the calorimeter where the tower dimensions are 8 cm x 8 cm. The width of this distribution is characteristic of the inherent spatial resolution achievable using the hadron calorimeter information with a small energy dependence. We have studied the rms deviation of several such distributions as a function of the incident hadron energy for the three different cathode pad sizes and have observed that the spatial resolution worsens as the pad size increases or equivalently as R, the distance from the beam axis, increases. At 100 GeV the dependence on pad size is expressed as σ=0.25d where σ is the spatial resolution and d is the pad dimension. In addition, at lower beam energy we noticed that the statistical fluctuations in the development of a hadron shower became important,

influencing our measurements of the shower center of gravity and hence giving rise to a worsening in the rms position resolution. At 40 GeV, for instance, the effect of the pad size on the spatial resolution is twice that at 100 GeV.

c) Transverse and longitudinal shower development

Using the signals from the surrounding cathode pad towers and the 27 individual anode wire planes, we investigated the spatial development of hadron showers in the calorimeter.

To study the longitudinal development of a typical shower in this calorimeter, we analyzed each event by first locating the plane in the system where the shower originated and calling this longitudinal position the origin of the shower. We recorded the energy deposited in each subsequent layer as a function of its distance from the origin of the shower. In order to study the average behavior for a typical shower we summed these distributions for many events of the same total energy. Figure 10 shows the results of these measurements for three different beam momentum settings. From this figure we see that the shower maximum occurs at approximately 1 interaction length into the calorimeter independent of the shower energy. Furthermore, the shape of the three longitudinal energy distributions can be described by a simple exponential function of the form $e^{-a_L \lambda}$ with the parameter a_L being a function of the incident energy. The results of our fits to the data gives values of $a_L = 0.58, 0.50$ and 0.43 inverse interaction lengths for the 40, 100 and 200 GeV data, respectively. From these shower shapes we calculate that the fraction of energy which leaks out of the downstream end of the calorimeter for these three beam energies is $2\%, 3\%$ and 4%, respectively.

The transverse shower shape was studied by measuring the fraction of the

shower energy appearing in cathode pads at varying distances from the center of gravity of a particular shower. Due to the inherent granularity of our cathode pad structure, we were able to smooth out these distributions by combining data from several spatially different runs. The transverse shower shape can also be described by a simple exponential function of the form $e^{-a_T\delta}$ where δ represents the transverse distance from the shower axis to the center of the cathode pad of interest. The data are consistent with a value of $a_T = 0.21\ cm^{-1}$.

d) Special runs

In addition to the measurements already described, we undertook to study the effects of a coarser steel sampling thickness on this calorimeter. To study the calorimeter with 10 cm sampling we disconnected every other chamber from the high voltage. The results of these data runs were consistent with our expectation that the energy resolution of such a system should worsen as the square root of the sampling thickness, t, of the calorimeter. This degradation in resolution in our case corresponds to a value of (σ/E) of 20% for hadrons of 100 GeV.

IV. WIRE AGING TEST

It is known that using alcohol mixed with various ionization gases in wire chambers extends the life of the chambers by preventing aging of the wires and by controlling the onset of glow mode discharge[9]. Thus far ethyl alcohol has been used by most experimenters. For the CDF forward/backward gas calorimeters we could not use ethyl alcohol because it dissolved the conducting epoxy used in construction of the chambers.

It was noticed that isopropyl alcohol did not dissolve this conducting epoxy.

When the epoxy was washed with isopropyl alcohol or was immersed in it for over a week, there seemed to be no degradation of its conducting properties. These observations suggested that the isopropyl alcohol could possibly be used to protect the chambers from aging. To investigate this possibility, we built a small prototype of the hadron calorimeter chambers and studied its response to an Fe^{55} source with the isopropyl alcohol mixed in the argon-ethane gas.

The prototype of the hadron calorimeter chamber was built identical to the actual chambers in every respect except that it had only one pad. The pulses from the wires were amplified and analyzed by a LeCroy qVt and, in addition, the pulses from the cathode pad were observed on an oscilloscope. We had the option of having no alcohol mixed with the 50%-50% argon-ethane gas, or changing the amount of alcohol being mixed with the gas by varying the temperature of the alcohol in the bubbler through which the gas mixture is routed. The temperature of the alcohol was controlled to an accuracy of $\pm$ 0.1^oC.

A second chamber was used to normalize the results from the test chamber in order to compensate for the gain changes due to the fluctuations in the atmospheric pressure. This chamber was run only with standard argon-ethane gas without alcohol and with the same Fe^{55} source used for the test chamber.

The pad pulse generated by the Fe^{55} source was observed on an oscilloscope by using an FET probe in order to measure the effect of alcohol on the time constant of the pad/conducting epoxy system. The RC time constant of these pulses before and after the chamber was aged by 0.3 coulomb of charge, while isopropyl alcohol was added to the gas mixture, was identical. The pulse height spectra from a wire before and after the aging did not differ. For these spectra the full width at half maximum was the same and there was no measurable drop in the pulse

height. Therefore, as observed by an earlier study[10], we do not see aging with our gas mixture to the level of 0.3 coulomb of charge. We should also note that the pad pulses and the wire signals did not change noticeably after we increased the high voltage to induce a glow mode of the chamber. These observations are clear indications of the fact that isopropyl alcohol prevents aging of the wires while not affecting the structure of the epoxy used in chamber construction.

We measured the gain change at a fixed high voltage as a function of the amount of alcohol in the gas. We changed the amount of alcohol by varying the temperature of the alcohol bubbler. In Figure 11 we plot the change in the gain, relative to the gain when no alcohol is in the gas, as a function of the vapor pressure of the alcohol. The points on this plot are for alcohol temperatures of -10^oC (the rightmost point), -5^oC, 0^oC, $+5^oC$, and $+10^oC$ (the leftmost point). The gain is observed to drop with increasing alcohol temperature, i.e. with increasing amount of alcohol in the argon-ethane gas. The measurements are normalized to the measurements from the second chamber in order to compensate for outside changes (like change in atmospheric pressure) which occurred during the test time span.

Acknowledgements

We wish to express our appreciation to all of our CDF colleagues at Fermilab and elsewhere who assisted us in our beam tests at M-bottom. We would like to give special thanks to H. Kautsky for his help in organizing the mechanical aspects of this test; A. David, N. Diaczenko and J. Buchholz for their invaluable contributions in the construction of these chambers at Texas A&M; C. Haber, M. Mishina, Y. Fukui, and S. Kim who helped us get started at M-bottom; M. Atac who contributed to the aging test; and the Fermilab rigging crews that helped

us in the installation and tear down of this test set-up. We would also like to acknowledge the assistance we received from the Harvard University and Brandeis University groups working on the CDF, in adopting their original electromagnetic calorimeter design to the CDF forward/backward hadron calorimeter system. This work has been supported in part by the U. S. Department of Energy contract DE-AS05-81ER40039.

REFERENCES

*) Permanent address, INFN, Torino, Italy.

1) "The Collider Detector at Fermilab", F. Abe et al. (Submitted to NIM).

2) This paper will present only the results of the early test beam and cosmic ray tests on this system. During the first data taking run with the Fermilab Collider a new phenomena was observed in this system due to the energy sampling fraction inherent in gas calorimeters. These events are characterized by small localized energy depositions in the calorimeter, which are interpreted as higher energy hadron showers. These events did not manifest themselves significantly in our early test beam data taking. We are presently carrying out a more extensive study of the origin and characteristics of these localized energy depositions in these calorimeters and our findings will be the subject of a future paper on this subject.

3) Minalex Corporation, White House Station, New Jersey.

4) Knobby Krafters, Attleboro, Massachusetts.

5) Philips Elmet Corporation, Lewiston, Maine.

6) Abatron Incorporated, Gilberts, Illinois. The conducting epoxy used in constructing the hadron calorimeter chambers was originally developed by the Harvard University group for the forward/backward electromagnetic calorimeter of CDF.

7) "CDF Front End Electronics: The RABBIT System", G. Drake et al. (Submitted to NIM).

8) For comparison, see the following articles for other hadron calorimeter results:

H.Abramowicz et al., NIM 180(1981), 429;

A.Beer et al., NIM 224(1984), 360;

M.J.Corden et al., Physica Scripta 25(1982), 11;

A.L.Sessoms et al., NIM 161(1979), 371;

C.W.Fabjan and T.Ludlam, Ann.Rev.Nucl.Part.Sci. 32(1982), 335 and references therein.

9) M. Atac et al., NIM 200(1982), 345.

M. Atac, IEEE Trans. on Nuclear Science, Vol. NS-31, No.1 (1984) 99.

M. Atac, Proceeding of the Workshop on Radiation Damage to Wire Chambers at LBL., Jan. 16-17, 1986.

10) M. Atac, IEEE Trans. on Nuclear Science, Vol. NS-34, No.1 (1987) 476.

FIGURE CAPTIONS

Figure 1 : A perspective view of one of the sections of the CDF forward/backward hadron calorimeter.

Figure 2 : Pad structure of a CDF forward/backward hadron chamber.

Figure 3 : Cross section of a CDF forward/backward hadron calorimeter cell.

Figure 4 : Chamber gain versus high voltage as determined from the cosmic ray data.

Figure 5 : Energy distribution for E_{beam} = 100 GeV. Smooth curve is the result of a Gaussian fit with <nep> = 25.0, N_{max} =183 and σ = 3.52 nep.

Figure 6 : Number of equivalent particle versus E_{beam}.

Figure 7 : σ/peak versus $1/\sqrt{E_{beam}}$.

Figure 8 : $(\sigma/\text{peak})\sqrt{E_{beam}}$ versus high voltage at 50 GeV.

Figure 9 : Distribution for a typical run of the distance between the center of gravity of the pad signals and the particle impact point projected by the beam MWPC.

Figure 10: Hadronic longitudinal shower distribution for E_{beam} = 200 GeV (circles), 100 GeV (crosses), 40 GeV (stars) versus the depth expressed in interaction length units.

Figure 11: Gas gain change versus alcohol vapor pressure at fixed high voltage.

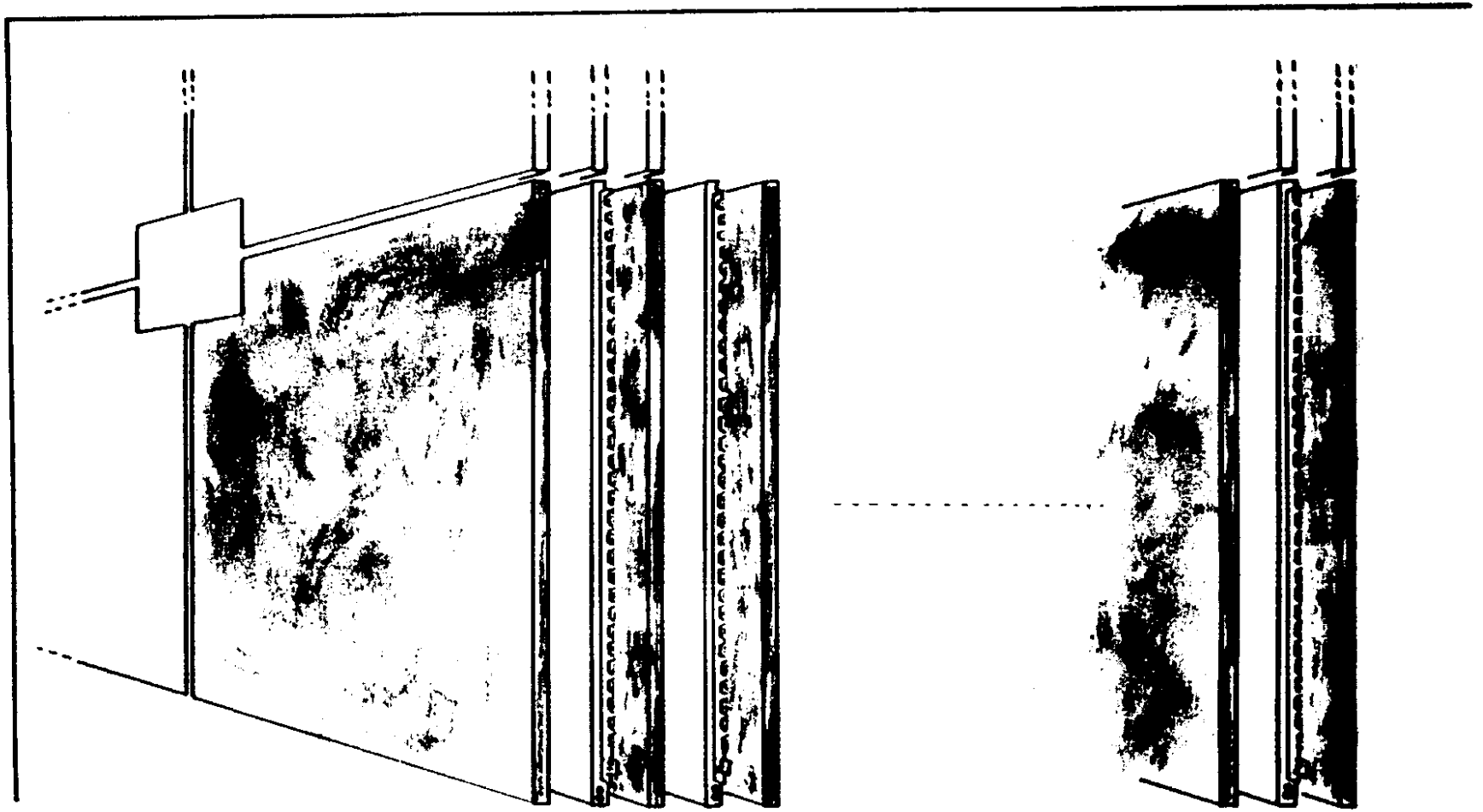

Figure 1

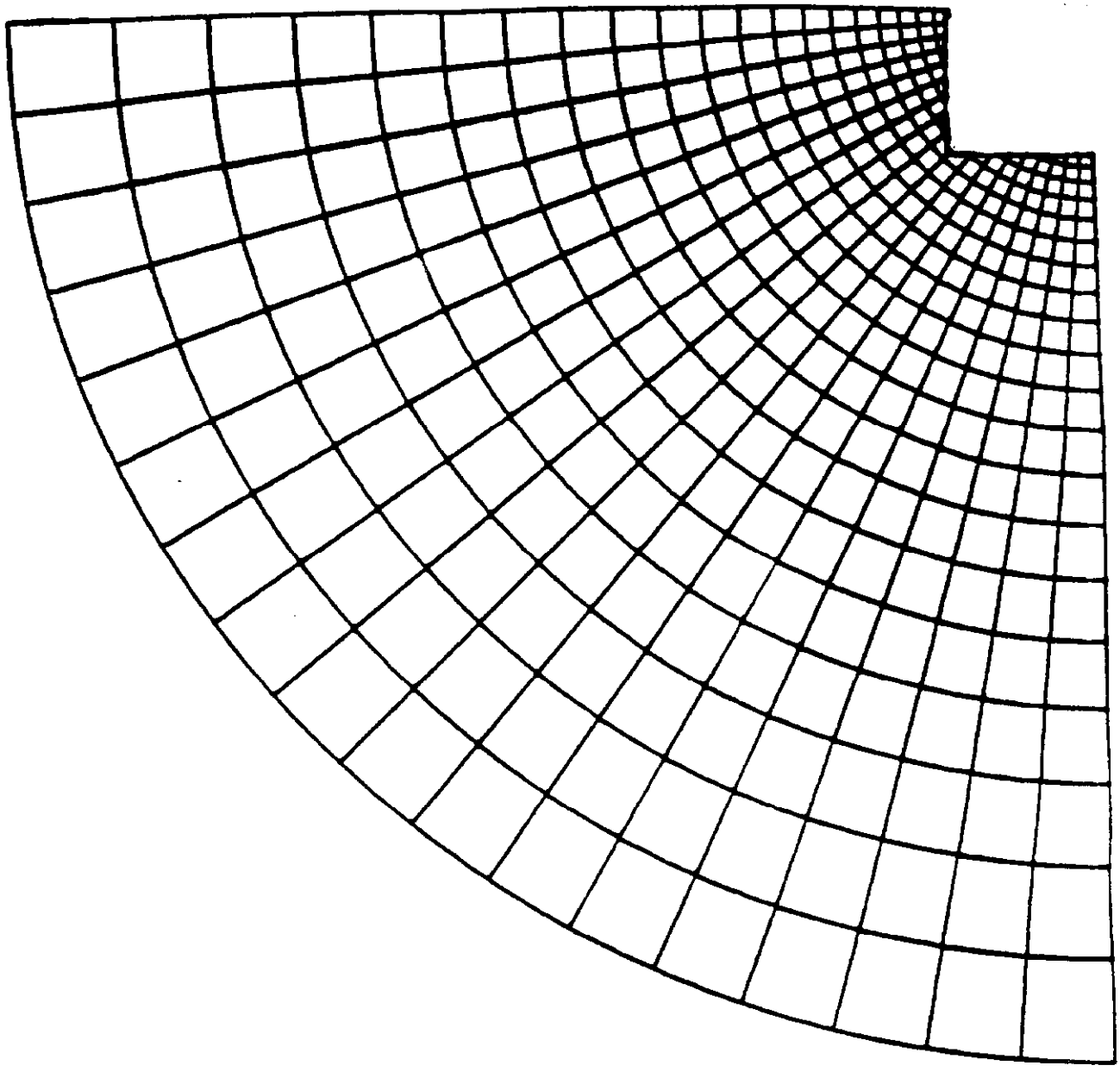

Figure 2

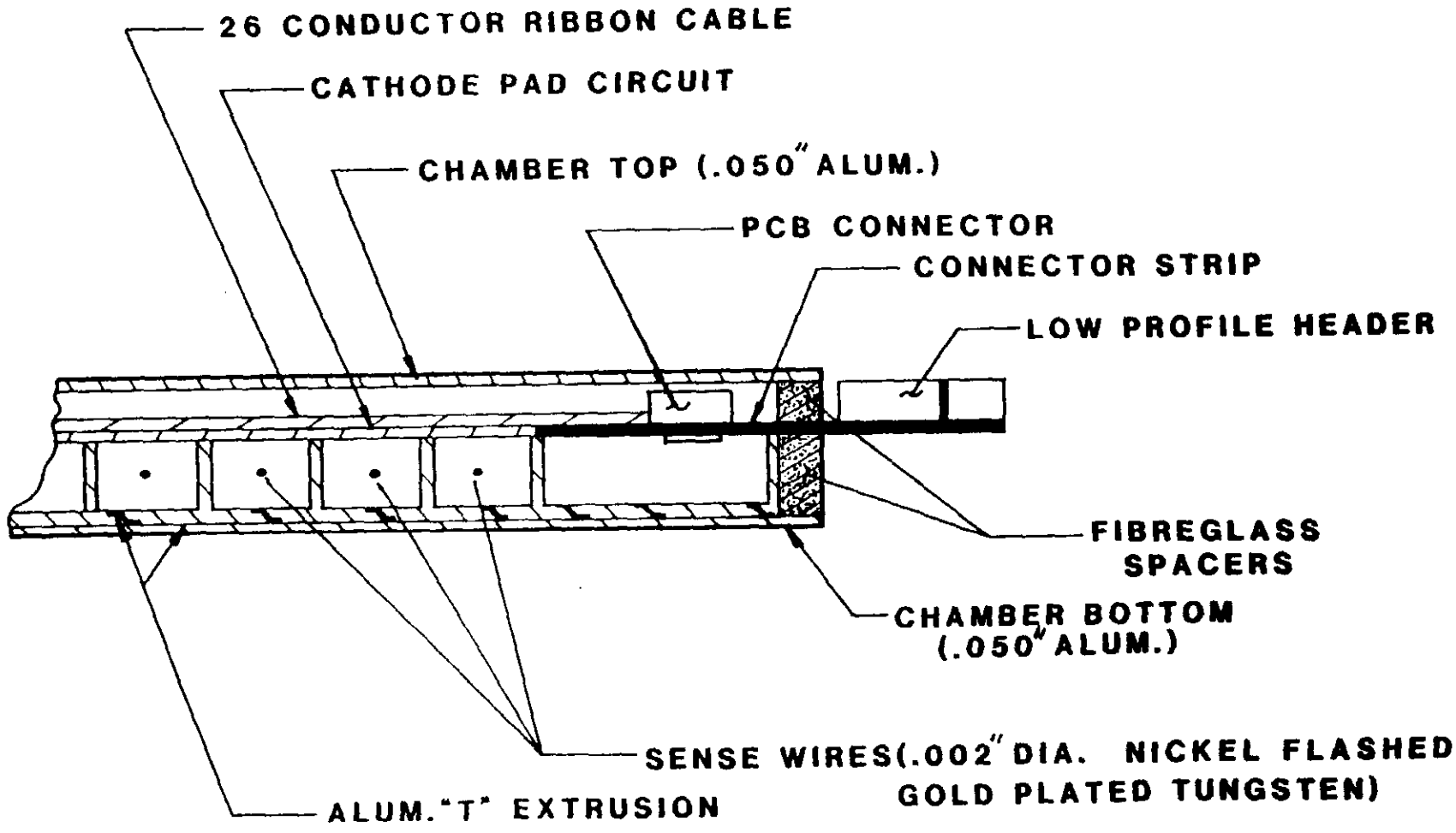
26 CONDUCTOR RIBBON CABLE
CATHODE PAD CIRCUIT
CHAMBER TOP (.050" ALUM.)
PCB CONNECTOR
CONNECTOR STRIP
LOW PROFILE HEADER
FIBREGLASS SPACERS
CHAMBER BOTTOM (.050" ALUM.)
SENSE WIRES(.002" DIA. NICKEL FLASHED GOLD PLATED TUNGSTEN)
ALUM."T" EXTRUSION

Figure 3

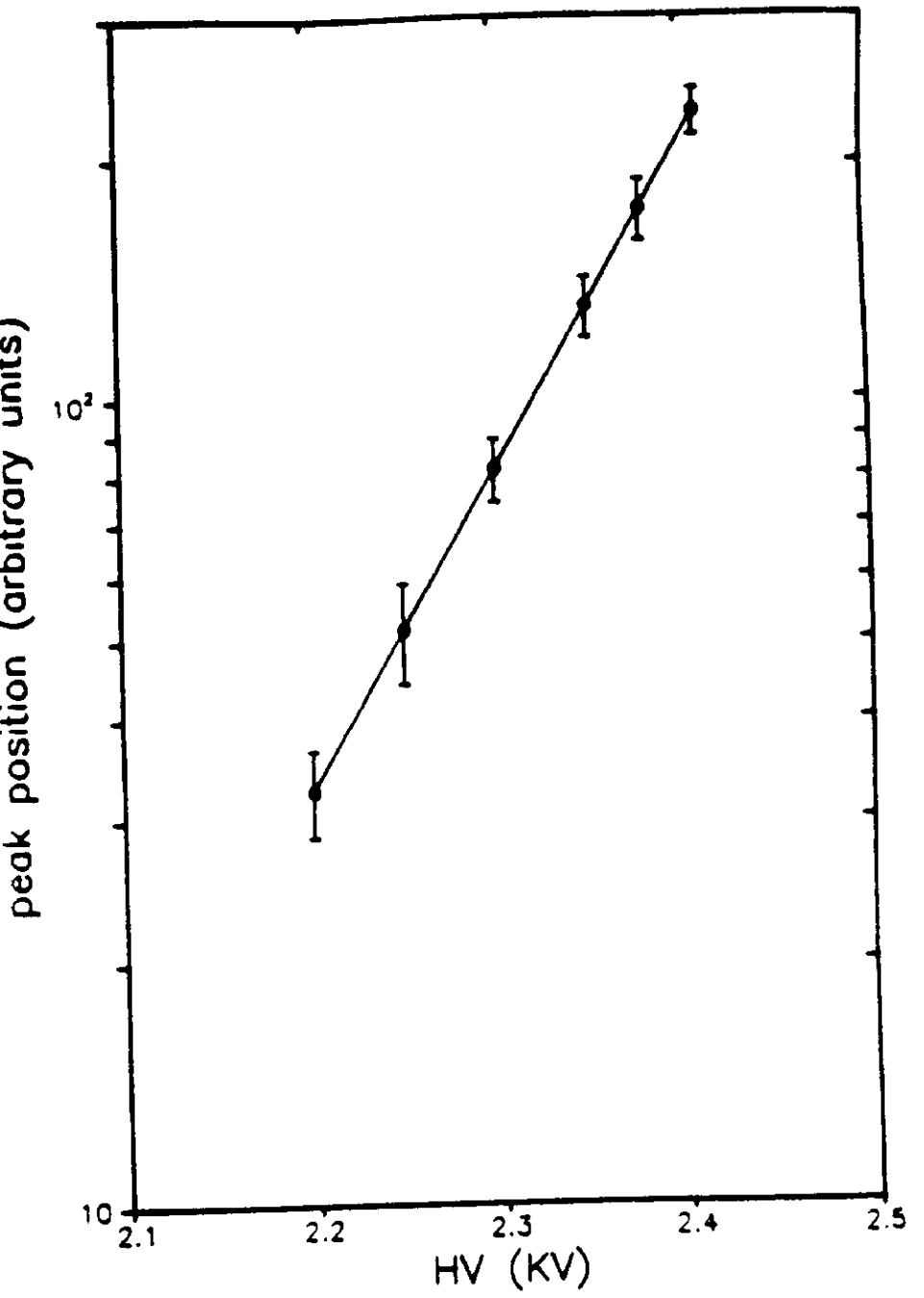

Figure 4

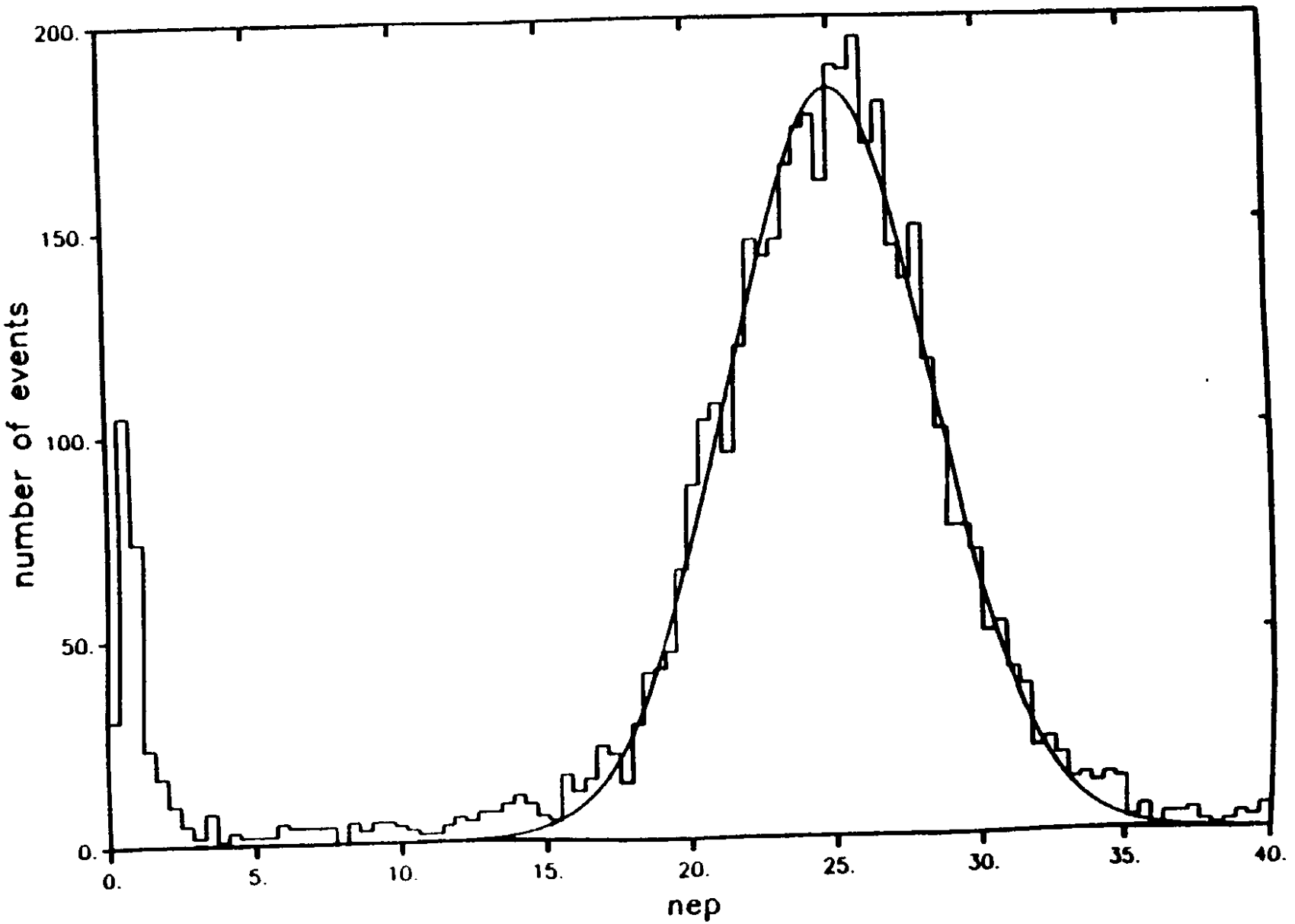

Figure 5

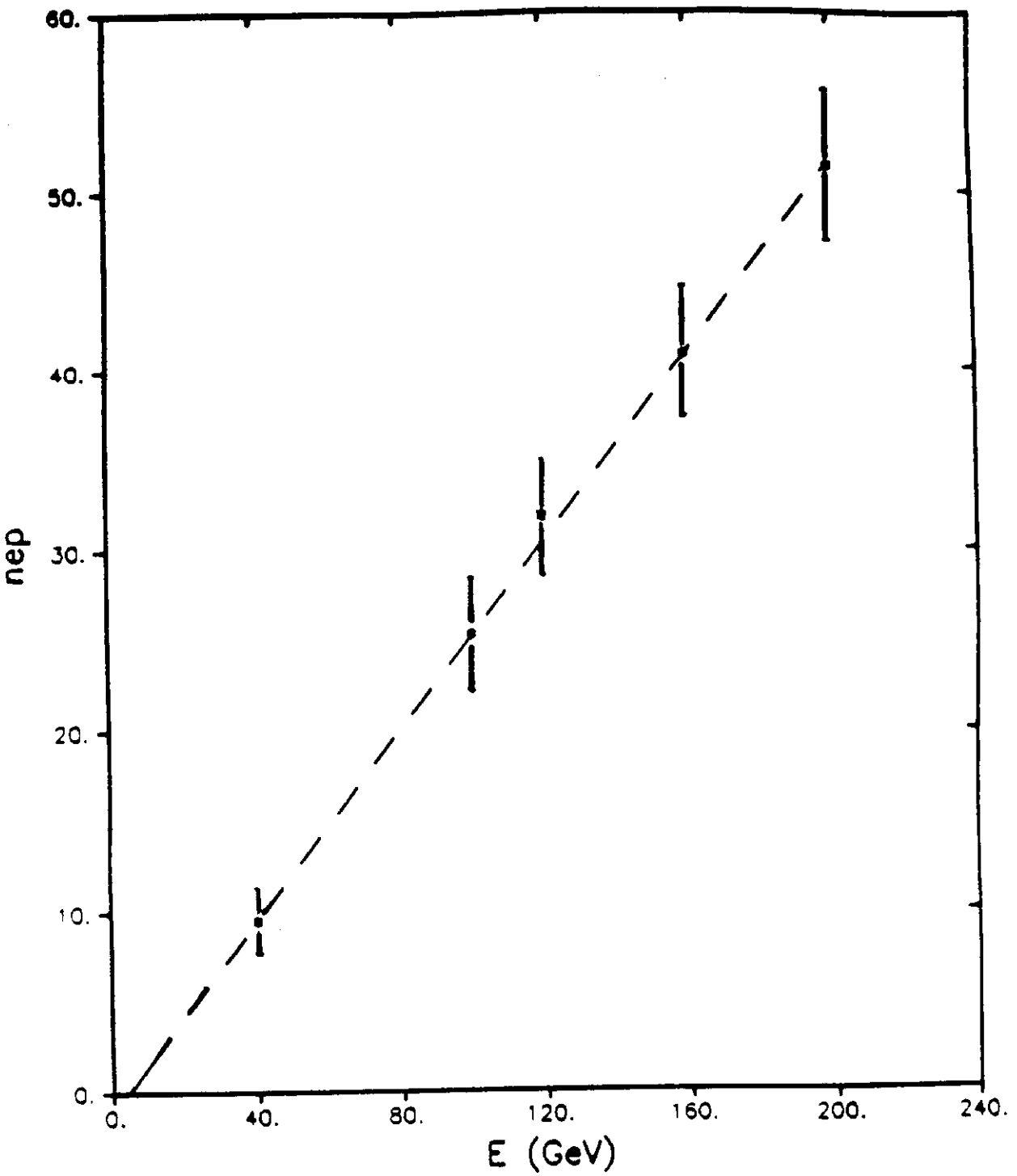

Figure 6

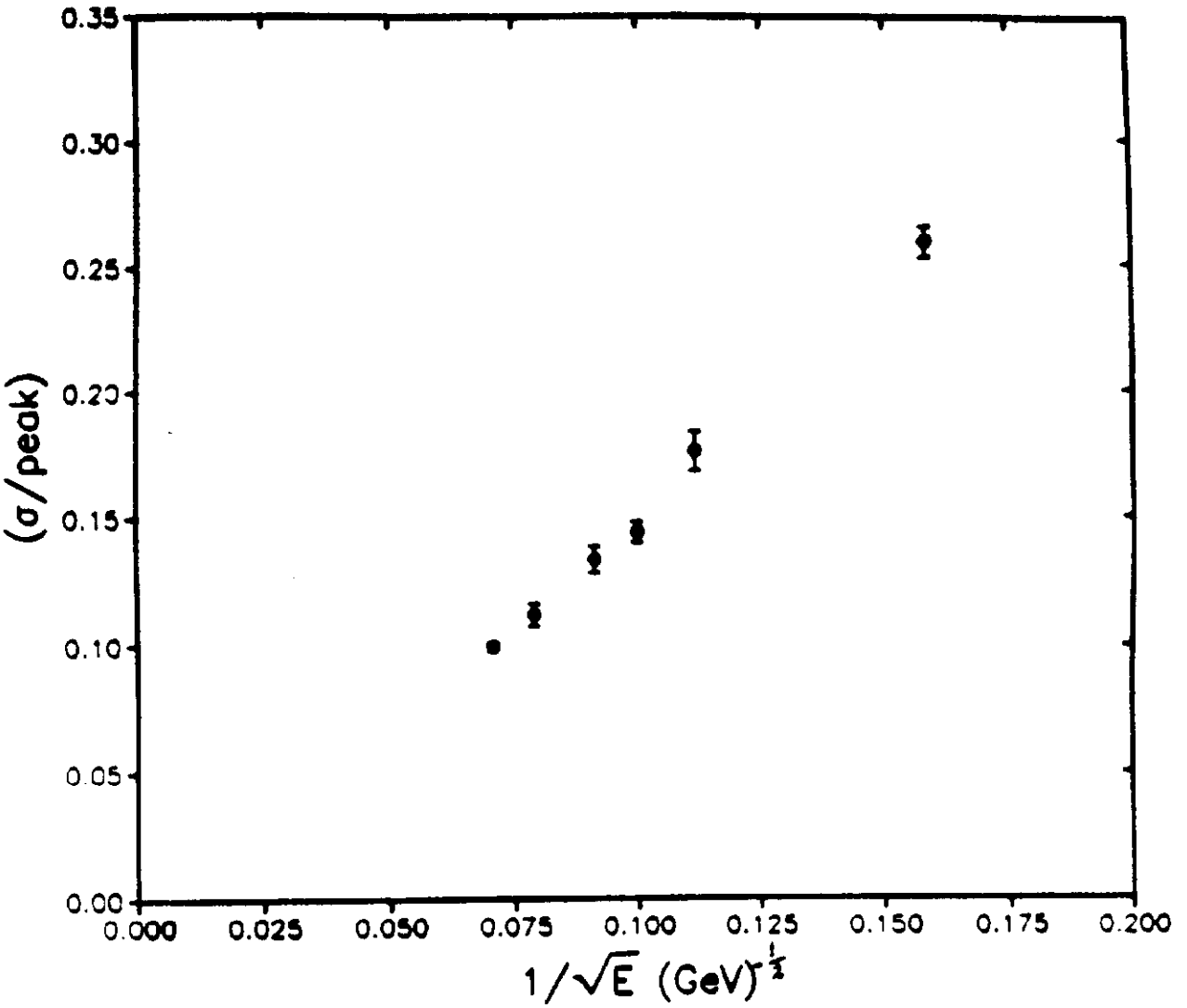
0.35
0.30
0.25
0.20
0.15
0.10
0.05
0.00
(σ/peak)
0.000
0.025
0.050
0.075
0.100
0.125
0.150
0.175
0.200
1/√E (GeV)^-1/2

Figure 7

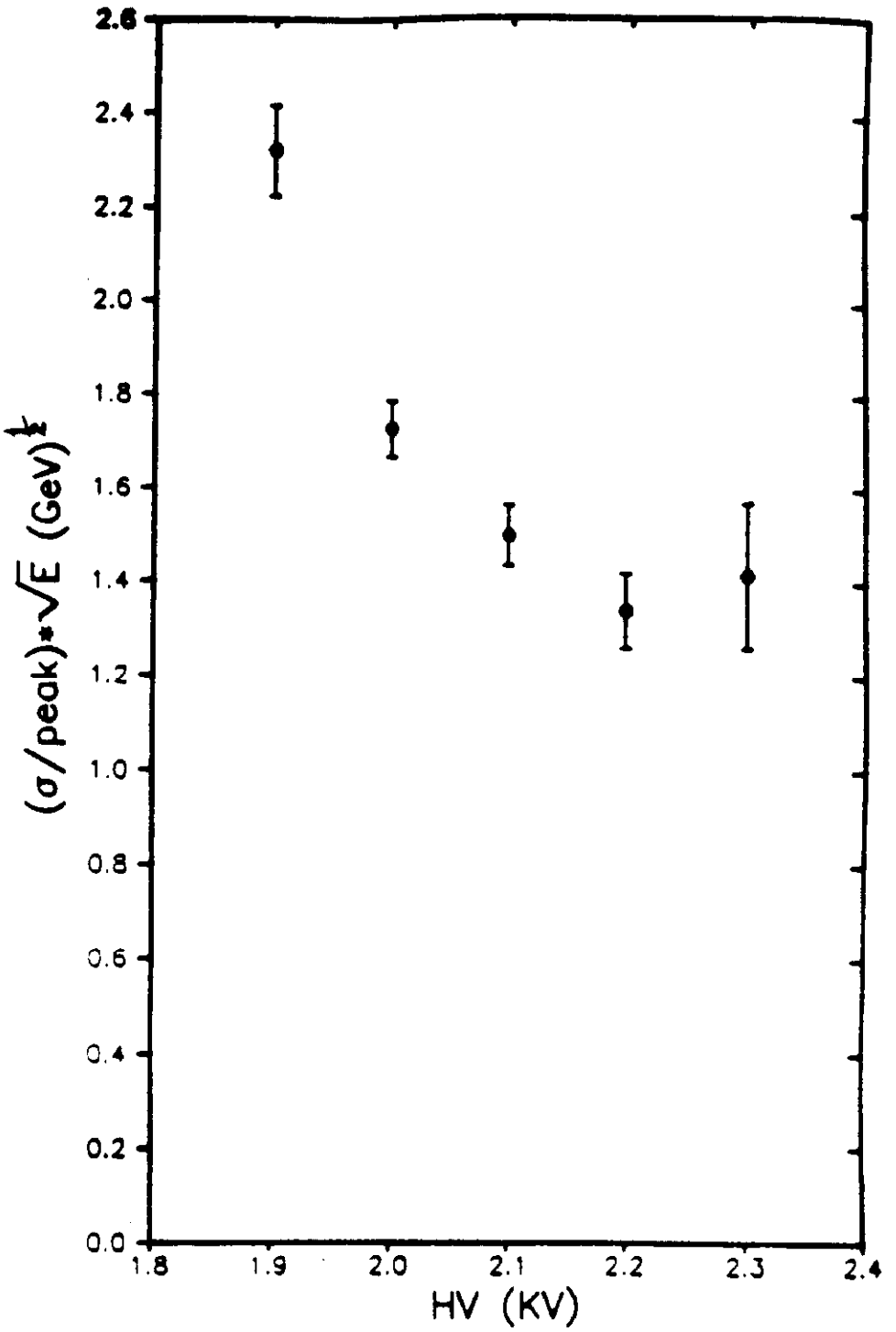
2.6
2.4
2.2
2.0
1.8
1.6
1.4
1.2
1.0
0.8
0.6
0.4
0.2
0.0
(σ/peak)*√E (GeV)^½
1.8
1.9
2.0
2.1
2.2
2.3
2.4
HV (KV)

Figure 8

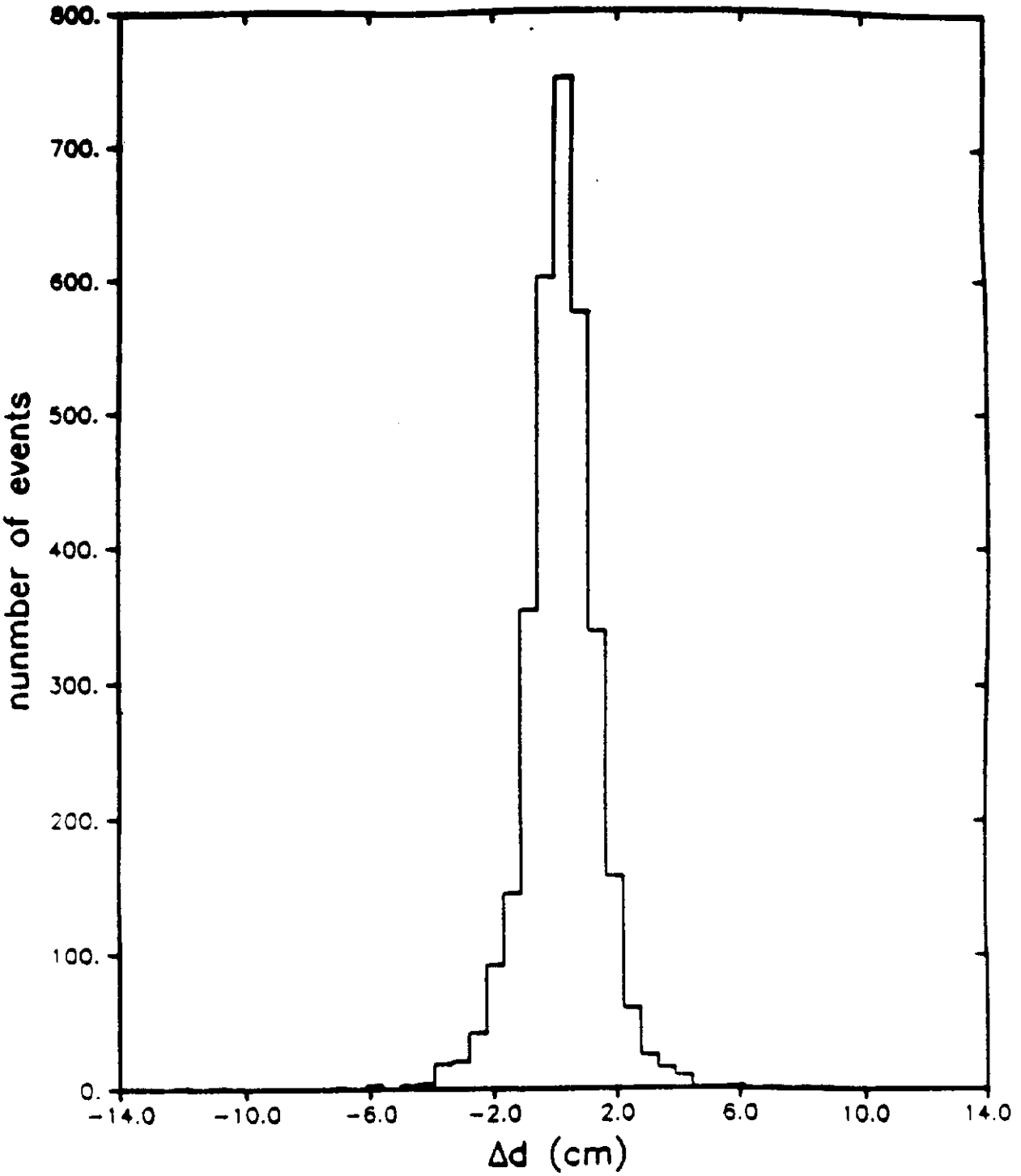
800.
700.
600.
500.
400.
300.
200.
100.
0.
nunmber of events
-14.0
-10.0
-6.0
-2.0
2.0
6.0
10.0
14.0
Δd (cm)

Figure 9

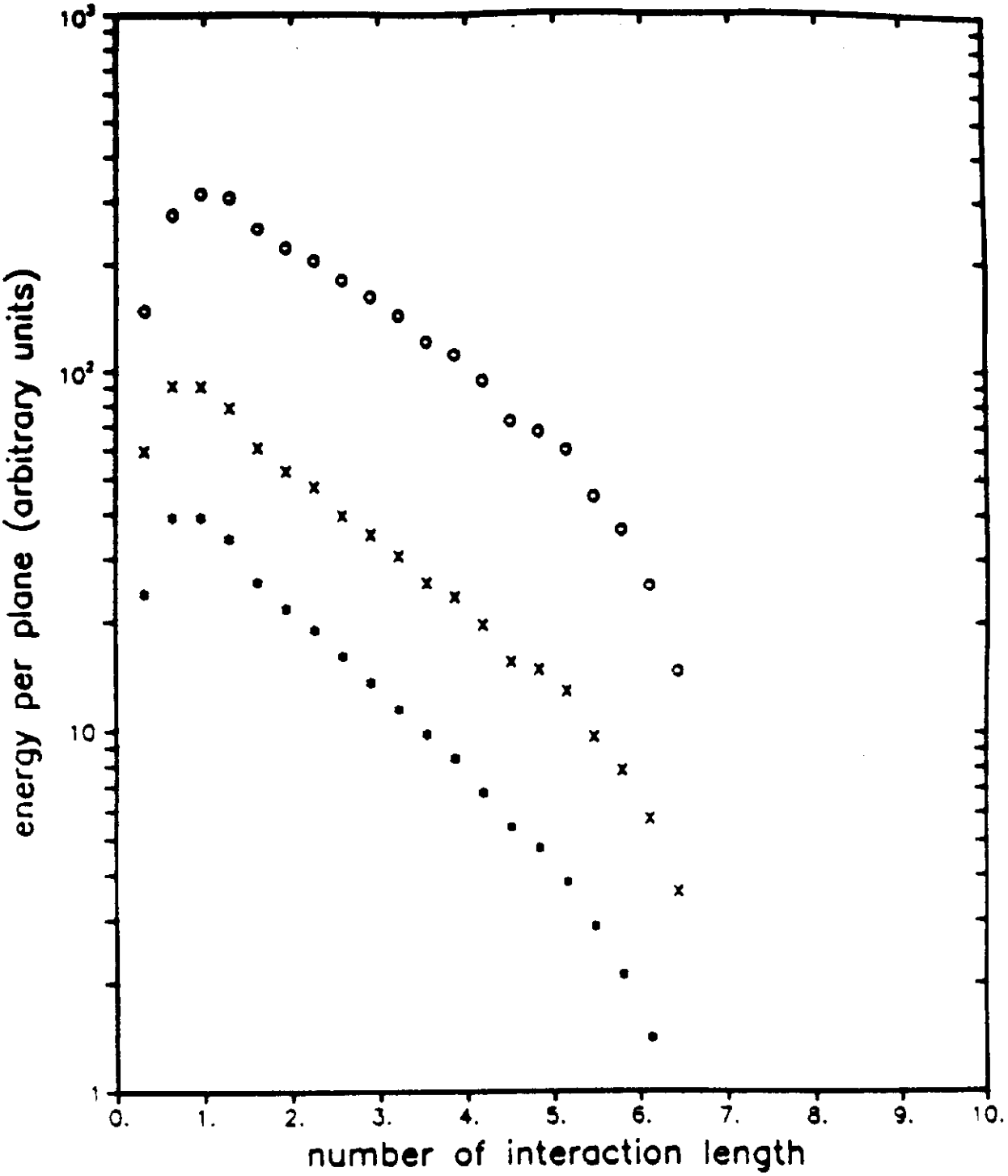
energy per plane (arbitrary units)
10^3
10^2
10
1
0.
1.
2.
3.
4.
5.
6.
7.
8.
9.
10.
number of interaction length

Figure 10

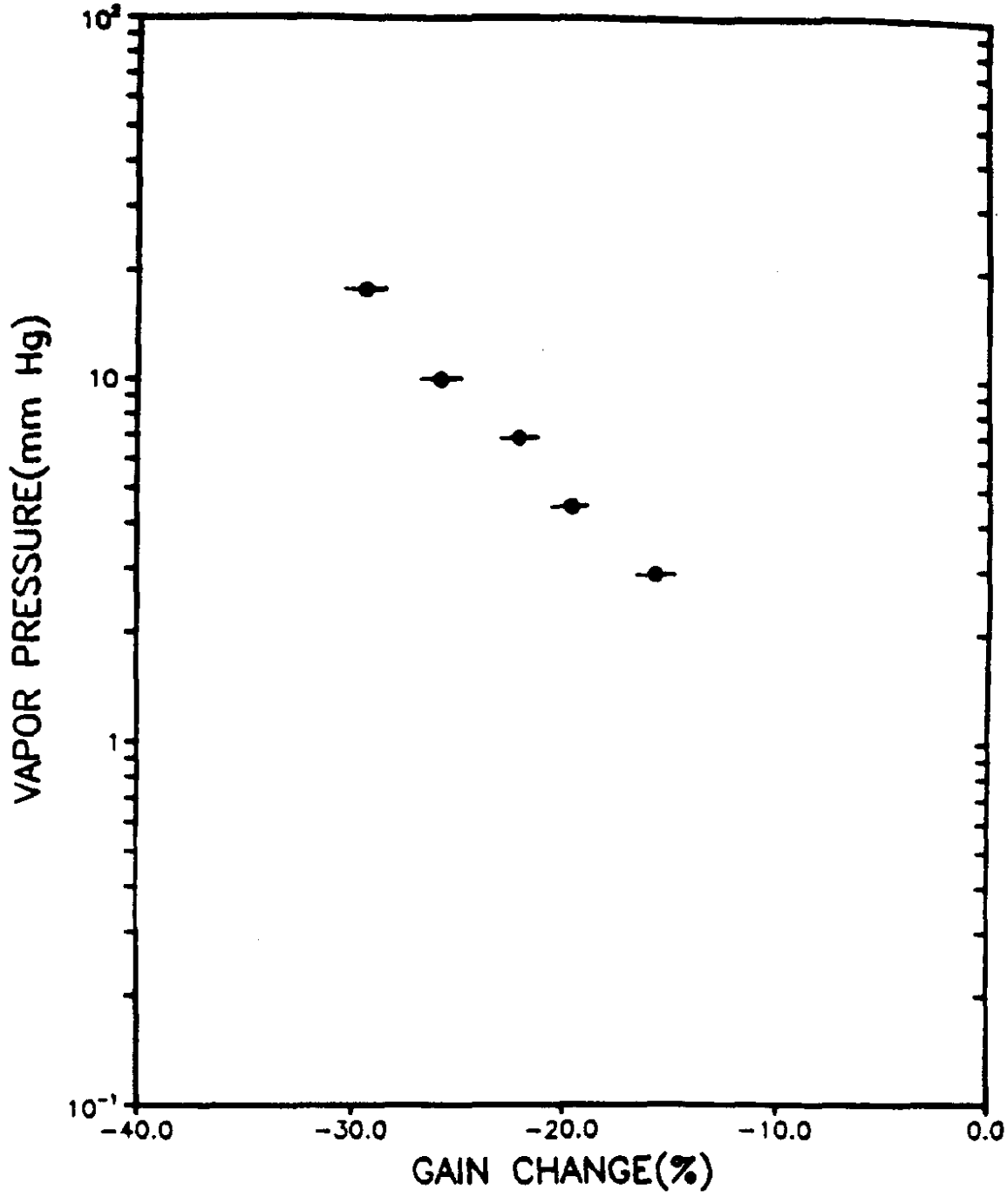

Figure 11